REPORT DOCUMENTATION PAGE

AFRL-SR-AR-TR-06-0056

1. REPORT DATE *(DD-MM-YYYY)*	2. REPORT TYPE	3. DATES COVERED *(From - To)*
	Final Report	01 Dec 2001 - 30 Nov 2005

4. TITLE AND SUBTITLE
Development of an Efficient Micro-Heal Exhanger: The Integration of Design, Processing and Testing

5a. CONTRACT NUMBER

5b. GRANT NUMBER
F49620-02-1-0025

5c. PROGRAM ELEMENT NUMBER

6. AUTHOR(S)
Patrick Kwon

5d. PROJECT NUMBER

5e. TASK NUMBER

5f. WORK UNIT NUMBER

7. PERFORMING ORGANIZATION NAME(S) AND ADDRESS(ES)
Department of Mechanical Engineering
Michigan State University
East Lansing, Michigan 48824

8. PERFORMING ORGANIZATION REPORT NUMBER

9. SPONSORING/MONITORING AGENCY NAME(S) AND ADDRESS(ES)
USAF/AFRL
AFOSR
875 N. Randolph Street
Arlington VA 22203 NA
Dr Byung-Lip Lee

10. SPONSOR/MONITOR'S ACRONYM(S)
AFOSR

11. SPONSOR/MONITOR'S REPORT NUMBER(S)

12. DISTRIBUTION/AVAILABILITY STATEMENT

Distribution Statement A. Approved for public release; distribution is unlimited.

13. SUPPLEMENTARY NOTES

14. ABSTRACT

Many new concepts in designing and fabricating thermal management materials (TMMs) were explored to make an efficient meso-scale heat exchanger. The proposed TMMs have multi-functionality that combines structural material with cooling components by utilizing embedded microstructures in a miniature-sized body to enhance heat and mass transfer, chemical reactions etc. 'Mesomachines' are expected to provide a number of important functions where a premium is placed on mobility, compactness, or point application. More specifically, we are designing and fabricating micro-textured (Functionally Graded Material (FGM)) and micro-configured (for cooling channels) medium to compensate thermal gradient loading as a result of heat transfer into a cooling fluid circulating in the network of channels and manifolds. Previous work [Kwon et al., 1994, Kwon and Dharan, 1995] attest to the motivation for such medium. For the complicated structure with cooling channels such as our heat exchanger, finite element (FE) modeling provides the flexibility needed to design an optimal gradiency in properties by analyzing not only the magnitude of heat transfer into the fluid flow but also the integrity of the structure..

15. SUBJECT TERMS

16. SECURITY CLASSIFICATION OF:			17. LIMITATION OF ABSTRACT	18. NUMBER OF PAGES	19a. NAME OF RESPONSIBLE PERSON
a. REPORT	b. ABSTRACT	c. THIS PAGE			19b. TELEPHONE NUMBER *(Include area code)*
U	U	U	UU	23	

Final Report

DEVELOPMENT OF AN EFFICIENT MICRO-HEAT EXCHANGER: THE INTEGRATION OF DESIGN, PROCESSING AND TESTING

Contract Number F49620-02-1-0025

Patrick Kwon
Department of Mechanical Engineering
Michigan State University
East Lansing, Michigan 48824
pkwon@egr.msu.edu
(517) 355-0173

EXTENTED ABSTRACT

Many new concepts in designing and fabricating thermal management materials (TMMs) were explored to make an efficient meso-scale heat exchanger. The proposed TMMs have multi-functionality that combines structural material with cooling components by utilizing embedded microstructures in a miniature-sized body to enhance heat and mass transfer, chemical reactions etc. 'Mesomachines' are expected to provide a number of important functions where a premium is placed on mobility, compactness, or point application.. More specifically, we are designing and fabricating micro-textured (Functionally Graded Material (FGM)) and micro-configured (for cooling channels) medium to compensate thermal gradient loading as a result of heat transfer into a cooling fluid circulating in the network of channels and manifolds. Previous work [Kwon et al., 1994, Kwon and Dharan, 1995] attest to the motivation for such medium. For the complicated structure with cooling channels such as our heat exchanger, finite element (FE) modeling provides the flexibility needed to design an optimal gradiency in properties by analyzing not only the magnitude of heat transfer into the fluid flow but also the integrity of the structure. Using a commercially available finite element (FE) package, ANSYS, the FGM body with the unidirectional channels through which water flows was modeled and an optimal gradiency in FGM properties is designed for a given steady state loading condition. In addition transient simulations were carried out to show the effectiveness of FGM. A series of processing techniques has developed to fabricate such multi-functional material and process models has implemented in the FE software, ABAQUS, to understand the processing parameters in compaction and sintering. Multi-layered FGMs practically undistorted by process-induced residual stress have been successfully fabricated. In processing, multi-layered FGMs practically undistorted by process-induced residual stress have been successfully fabricated with the channels. In addition, the residual stress in the fabricated FGM has been measured. Another important processing technique is to introduce the channels in the FGM body by embedding the fugitive phase. During the presitering stage, the fugitive phase burns out leaving the cavity in a shape of channels. This development can bring about the realization of other meso-scale devices such as micro-mixing channels, meso-combustion engine and meso-turbine.

1. Design of FGMs

FGMs are fabricated by spatially varying the compositional ratio between two powders, which is used as a medium in our efficient meso-scale heat exchanger. The channels for cooling fluids were introduced by compacting and sintering the powder with the fugitive phase in a shape of channel, which burns out during sintering. Based on the processing capability developed, the FGM body with channels shown in Figure 1 is specifically designed for steady state and transient loading conditions using coupled fluid-thermal-structural finite element analysis using ANSYS Multiphysics 9.0. The Mori-Tanaka scheme is used to estimate the effective properties such as elastic stiffness, coefficient of thermal expansion and thermal conductivity in FGMs. In the design of FGM, the gradient properties must be designed based on the loading condition to minimize thermal stresses in the heat exchanger. The physical dimensions of the disc-shape finite element (FE) model of the heat exchanger include the thickness of 6mm and the diameter of 19mm. For the preliminary design, we have assumed the cross-section of the channels be 2mmx1mm. A heat flux, Q, of 250kW/m^2 enters through its bottom surface. Water flows in all four channels with an inlet velocity of 0.5 m/s along the length of the channels. The water is discharged at the outlet to the ambient at atmospheric

pressure. The ambient air is assumed to be at 25°C and its convective heat transfer coefficient is approximated to be 60 W/ m² /K. The design objective is to minimize the induced thermal strain in the body under steady state as well as transient conditions.

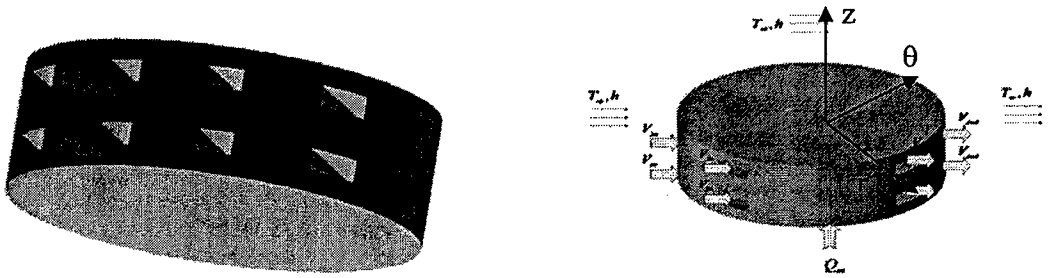

Figure 1: The FE Model of heat exchanger with cooling channels (side view and front view of the heat exchanger with 8 cooling channels)

To design an optimum FGM for the proposed heat exchanger, the thermal stress under a given loading can be examined in relation to the gradient properties. The thermal stresses as a function of layer thicknesses for three-layered and six-layered FGMs were studied. For the three-layered FGMs, the bottom layer (layer 1), through which the heat enters the FGM body, was alumina, followed by a mixture of 50% alumina + 50% zirconia (layer 2), and finally the top layer of pure zirconia (layer 3). The six-layered FGMs consists of, starting from the bottom layer, 100% alumina (layer 1), 80% alumina + 20% zirconia (layer 2), 60% alumina + 40% zirconia (layer 3), 40% alumina + 60% zirconia (layer 4), 20% alumina + 80% zirconia (layer 5) and 100% zirconia (layer 6). As demonstrated in Fig. 2, a variety of gradient properties can be achieved by varying the thicknesses of each layer while keeping the properties of each layer the same. For both three-layered and six-layered FGMs, three models have been analyzed; Model 1 represents FGM with each layer having the same thickness, Model 2 has a thicker zirconia (top) layer and Model 3 has a thicker alumina (bottom) layer. The thermal stresses of each model were studied under the steady state condition. The boundary condition used in the simulation is free, meaning no mechanical constraints.

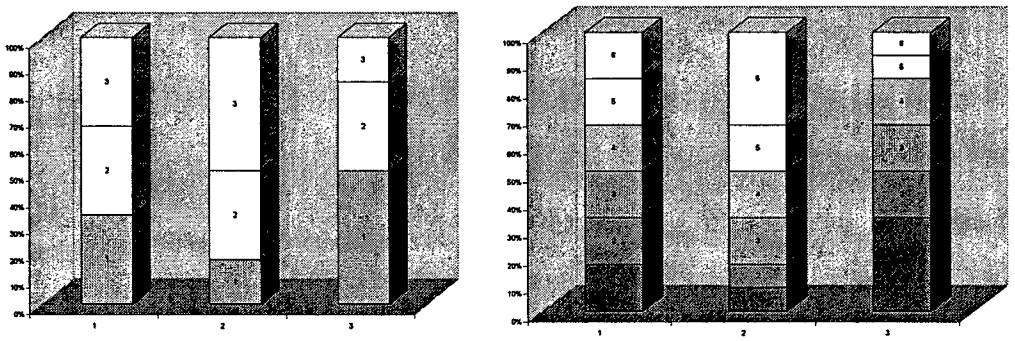

Model 1, Model 2 and Model 3 Model 1, Model 2 and Model 3

Figure 2: Various Layer Thicknesses for three-layered and six-layered FGM Models

Under these boundary condition, the results of the FE simulation show that the FGM with six layers and the gradient property resulting from Model 3 is more effective in reducing thermal stress. The results of FE simulation are shown with maximum principal stresses

at the center of the body ($r=0$ and $\theta=0$) in Figures 3, 4 and 5 as a brittle material such as ceramics are assumed to fail according to Rankine failure criterion. Figure 3 shows the comparison among homogeneous material (Alumina), three-equal (Model 1) layered FGMs and six-equal (Model 1) layered FGMs. The fact that FGMs with six equal layers reduce the thermal stresses implies more gradual changes in properties reduce the steady state thermal stress. Figure 4 shows the maximum principle stresses among the three models for three-layered FGMs while Figure 5 shows the maximum principle stresses among the three models for six-layered FGMs. Therefore, Model 2 of the six-layered FGM is most effective among the models considered in reducing steady state thermal stress for the given condition. The finite difference approach was used to validate our FE result. However, the results are sensitive to the boundary condition used. Figure 6 shows the simulation results with the bottom surface constrained only in z-direction, allowing the displacements in r and θ directions (see Fig. 1). Because of this boundary constraint much more restricted that the previous boundary condition, the stresses observed from the simulation were much higher. In this case, the gradiency provided by Model 3 is more effective in reducing the thermal stress. This emphasizes the importance in considering the concept of material-by-design in the application of FGMs

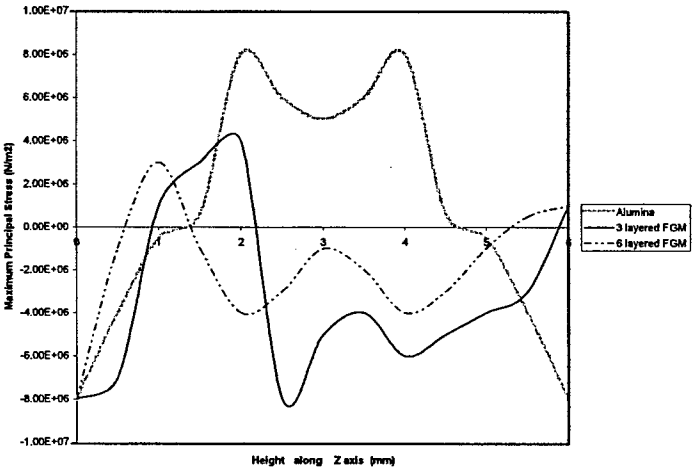

Figure 3: Maximum principal stresses at the center

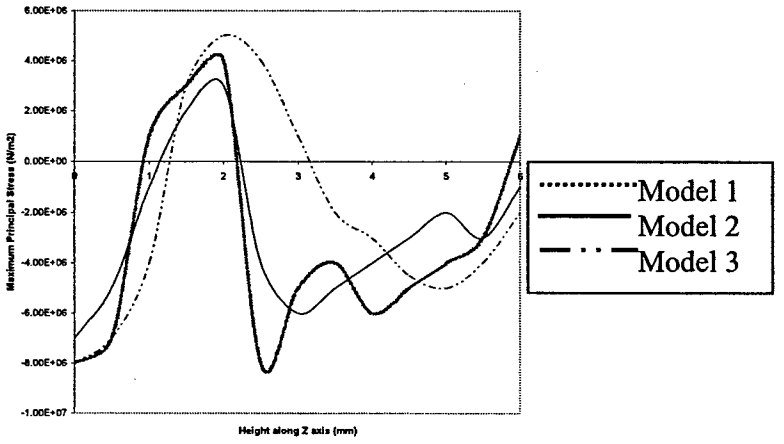

Figure 4: Maximum principal stresses for Three-layered FGMs at the Center

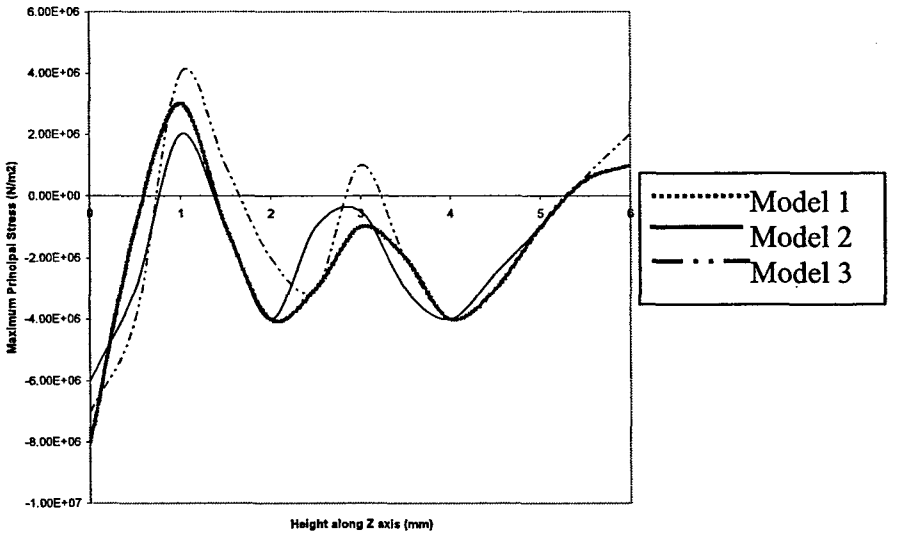

Figure 5: Maximum Principal Stresses for Six-layered FGMs at the Center

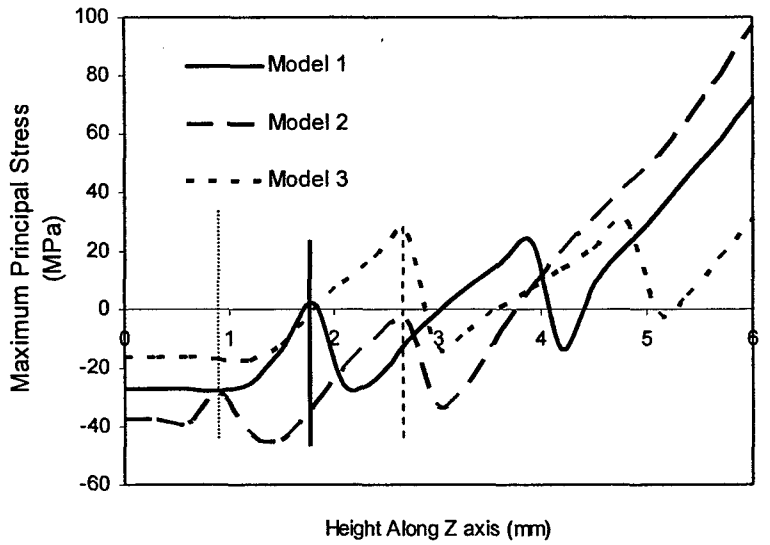

Figure 6: Maximum Principal Stresses at the center with the bottom face constrained in z direction.

The latter boundary condition was also used to build the transient FE Model using ANSYS Multiphysics 9.0. Following steps were taken:

i. 3D CFD/Flotran model with applied heat flux and no water flowing through channels was solved in transient case. The temperature of bottom layer near fluid channels was monitored. Limiting temperature rise near channels was 100°C.

ii. Water flow through channels was added to the CFD/Flotran model attained in the step i. The CFD model was solved for steady state analysis and temperature results were stored for next stage problem.

iii. A corresponding 3D structural model was generated for performing thermal stress/strain analyses. The temperature results from CFD/Flotran analysis from the step ii were applied on the nodes of the structural model.

The choice of a transient condition is important in evaluating the final result. Intuitively the stresses during normal transient conditions will not be as high compared to the steady state cases under the normal heating from the bottom side as the thermal gradient will gradually increase to its maximum value at the steady state. Therefore, we have to consider other transient conditions that are possible during the operation of the heat exchanger. One transient case that will exacerbate the state of stresses is when the cooling water started to flow after the temperature has already breached into the FGM body. However, because the water is assumed to be the coolant, we have simulated the maximum time for the stagnant water to reach the boiling temperature. With the heat flux of 250kW/m², the time to boiling to occur is 15 sec, after which the water started to flow. The stresses increase after 15 sec., reach the maximum and eventually drop down.

For all three models, the induced thermal stresses were within the maximum permissible stress limit. Figures 7 and 8 show the resulting maximum and minimum principal stresses from our transient analysis on Model 3 at t=19 sec. The difference between maximum and minimum principal stresses is 93.7MPa which occurs on the left wall of the far left bottom channel. Figures 9 and 10 show the stress at that location gradually increases and reaches the maximum values at t=26 sec.. The difference between maximum and minimum principal stresses is 226MPa. This value is still way below 355MPa which is the flexural strength of alumina reported in literature. Even though due to the space constraints, the temperature contours have not been presented, at t=26sec. the maximum attained temperature in the FGM medium was lowest at 191°C in Model 1, followed by 199°C and 236°C for Model 3 and Model 2, respectively. These high temperatures are reasonable due to the initial heating up when water was not flowing through channels. Figures 8 and 9 were plotted for minimum and maximum principal stresses at cross-section near one of the fluid channels (x=3.5mm y=0). These results are 0.2 mm away from the left wall of the second right bottom channel. The choice of this location is mainly due to the software constraints. Figures 11 and 12 shows that stresses reach their maximum value at t=19 sec. After that, the stress values gradually decrease down towards steady state values.

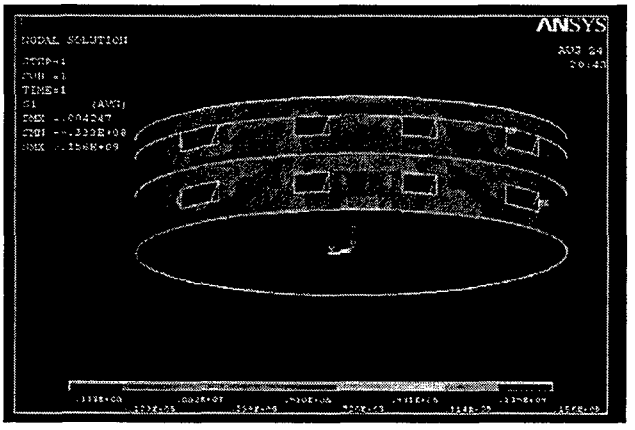

Figure 7: Maximum Principal Stress contour at t=19 sec.

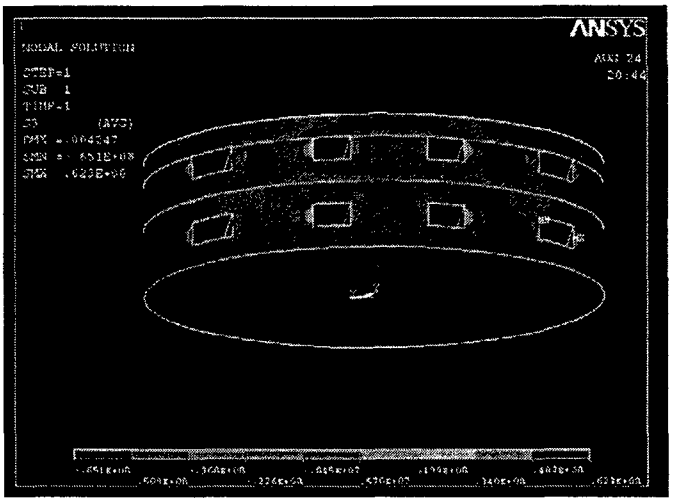

Figure 8: Minimum Principal Stress Contours at t = 19 sec.

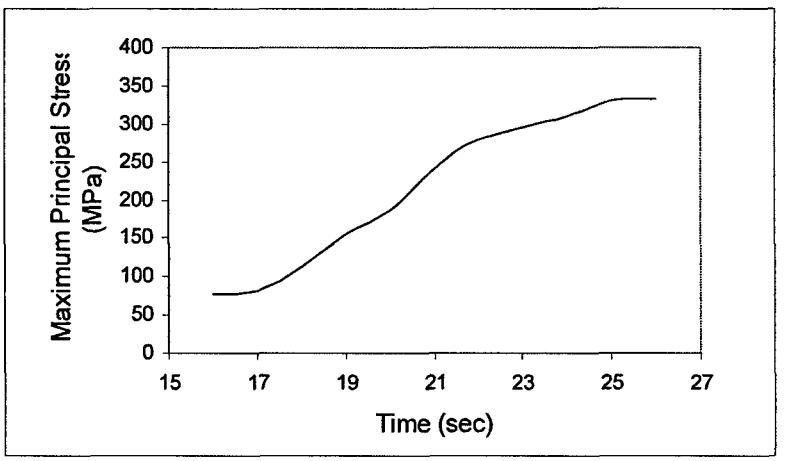

Figure 9: Maximum Principal Stress as a function of time

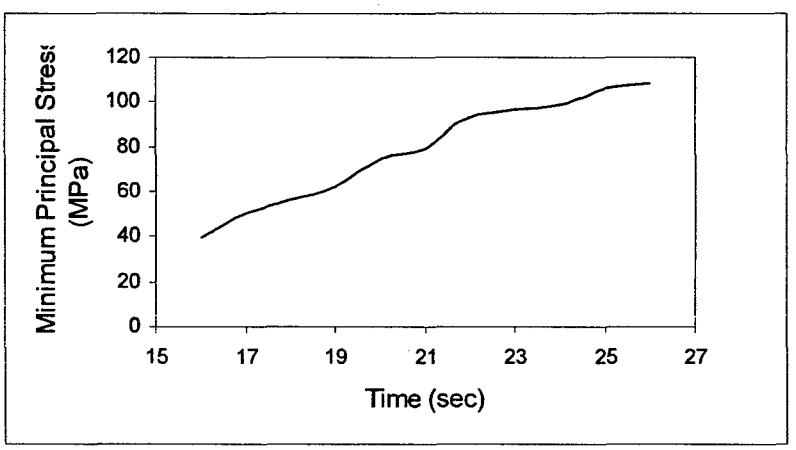

Figure 10: Minimum Principal Stress as a function of time

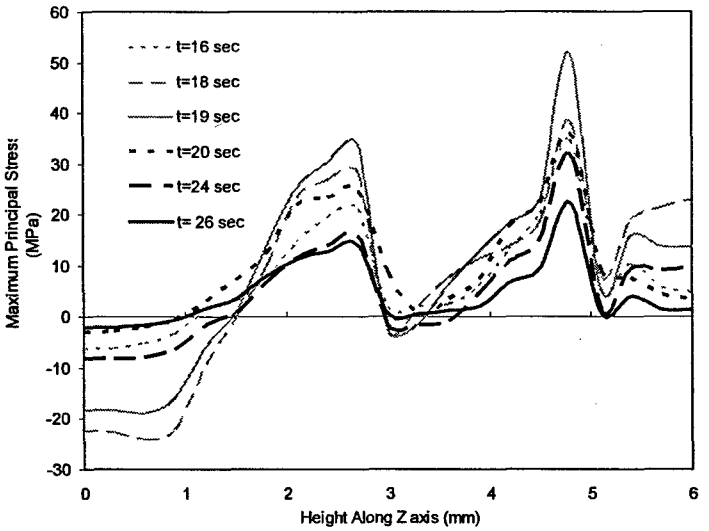

Figure 11: Maximum Principal stresses at x= 3.5, y=0

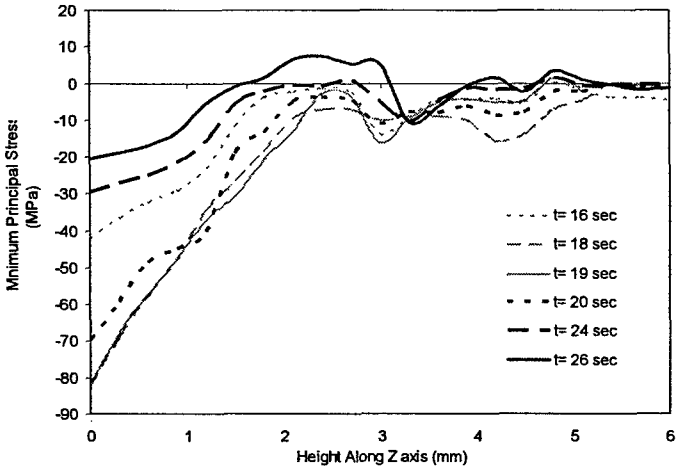

Figure 12: Minimum Principal stresses at x= 3.5, y= 0

2. Compaction and Sintering Models

One major problem in processing ceramic powder is the non-uniform relative density distribution and the residual stresses induced during compaction and sintering. The local densities and residual stresses are hard to measure experimentally. Thus, process simulation is necessary. Additionally, in the processing technique developed during the course of this research, the internal cavities are introduced by embedding a fugitive phase within the powder compact during compaction. During sintering the fugitive phase burns off and leaves the channels. To understand such process better, finite element models for both the compaction and sintering processes are developed using ABAQUS, which allows us to simulate before experiments.

Compaction models are developed based on theory of plasticity using the modified Drucker-Prager/cap model from soil mechanics. Because the powder is considered to

have non-associative flow rule, both plastic flow potential (G) and the yield surface (F) must be determined through experiments. The yield surface, which consists of F_t, F_c and F_s, and the plastic flow potential are assumed to be a function of hydrostatic stress (p), deviatoric stress (q) and relative density (D). Both G and F are presented in Figure 13. Each model has an associative cap-shape and a non-associative linear yield surface in the meridional (p-q) space. The cap yield surface models hardening of ceramic compact during triaxial loading whereas the linear yield surface models the ceramic compact behavior during shear loading. The modified Drucker-Prager/cap model allows for softening or plastic dilation to occur during shear yielding.

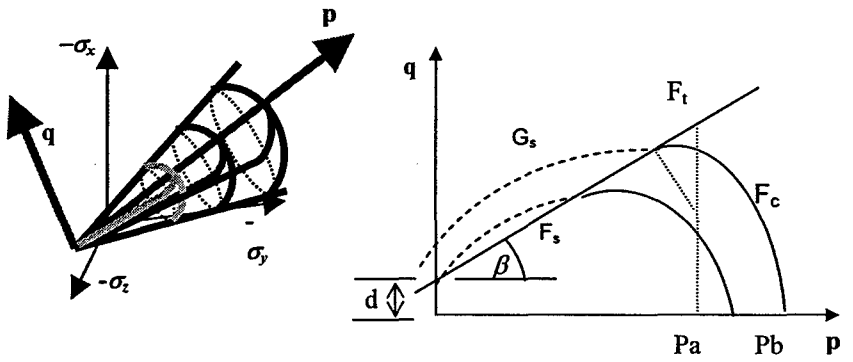

Figure 13: Yield Surface and Plastic Flow Potential

The constitutive laws can be summarized by the following equations

$$\underline{\sigma} = \underline{C}^e \underline{\varepsilon}^e = \underline{C}^e (\underline{\varepsilon} - \underline{\varepsilon}^p),$$

$$F = f(p, q, D) = 0,$$

$$\underline{\varepsilon}^p = \lambda \frac{\partial G}{\partial \underline{\sigma}}$$

where $\underline{\sigma}$ is the stress, $\underline{C}^e$ is the stiffness, G is the plastic potential, ε , $\underline{\varepsilon}^e$ and $\underline{\varepsilon}^p$ are the total, elastic and plastic strain, respectively. Empirical material parameters can be obtained in open literature. This compaction model allows for the prediction of relative density and residual stress distributions within a ceramic compact, which is difficult to obtain experimentally and essential in understanding the compaction process.

Depending on the size and shape of the fugitive phase as well as the magnitude of applied load, some powder will not be compacted uniformly throughout the compact. The density gradients are claimed to be responsible for the premature crack. Thus the powder compaction has been simulated with arbitrary shapes of fugitive phase. Based on our 3-dimensional simulation of the compaction in our cylindrical die, we have found that the plane strain condition is adequate to model the density distribution around the fugitive phase. Figure 14 shows the density distribution with the fugitive phase with the square cross-section in plane strain condition. Three cases, A, B and C, were shown to illustrate the orientation and location of the fugitive phase. The case A shows the least density gradient while the case C shows the highest density gradient in the compact. This is demonstrated in our experimental compaction as the case C samples have consistently cracks even at a relatively low load. However, the results are based on the

constitutive models of zirconia gathered in literature as we have not conduct the experiments on the powders used in this study.

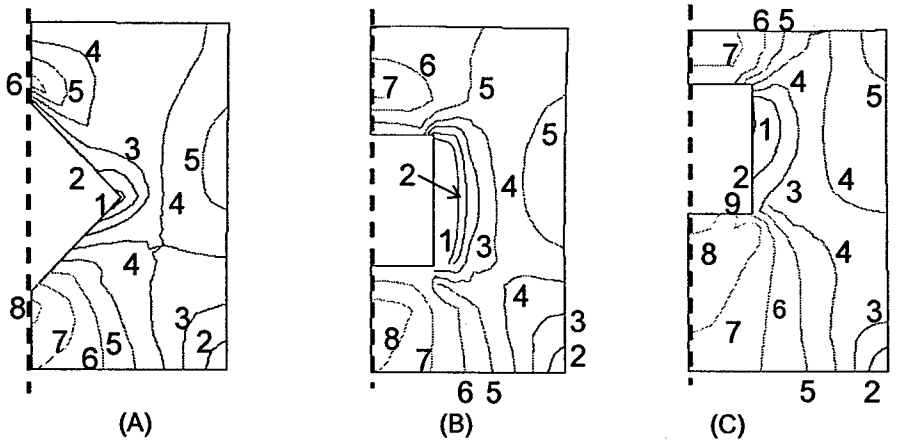

Figure 14: Relative density distribution after ejection simulated after subjecting to 23 MPa of axial pressure. A graphite piece is embedded in different orientations and locations as in (A), (B) and (C). The graphite piece has a cross-section of 2 mm X 2 mm.

A finite element model for sintering process based on viscoplasticity constitutive law is developed following the development made by as Kim et al, [2001]. The sintering process is assumed to consist of a densification stage and a grain growth stage. The sintering constitutive model developed by Kwon et al. [1996] is adopted. This model assumes two distinguishable modes in sintering, namely shear deformation and densification, as summarized below:

$$\dot{\varepsilon}_{ij}^{pl} = \frac{s_{ij}}{2\mu_p} + \frac{1}{3K_p}(-p - \sigma_s)\delta_{ij},$$

where $\dot{\varepsilon}_{ij}^{pl}$ is the plastic strain rate, s_{ij}, p, and σ_s the deviatoric, hydrostatic and sintering stress, respectively. μ_p and K_p are the shear and bulk viscosities, each of which are a function of initial relative density, current relative density, grain size, temperature, sintering potential, sintering period, any applied load if present and material properties such as coefficients of diffusion and atomic volume. Most constitutive models found in the literature differ only in the modeling of shear and bulk viscosities. With regard to grain growth, a simple model is adopted, whose material parameters are determined from observing grain sizes evolution with sintering time using scanning electron microscope. In this work, pressureless sintering experiments are performed to obtain empirical curve-fit parameters needed in the sintering model. Parameters not obtained experimentally are adopted from the literature.

Both compaction and sintering models have been implemented in commercially available Finite Element Code, ABAQUS. The results from FE simulation are consistent with findings of other researchers [Aydin et al., 1996; Kwon and Kim, 1996; Kim et al., 2000 and Zipse, 1997] are in agreement with our experimental observations in making various features in our meso-scale heat-exchanger. The compaction models show that the sites yielding in shear during top punch removal and continue yielding during ejection

to coincide with micro-crack sites in real specimen, whereas the sintering model implies that sintered products are more uniform in their final relative density and residual stress distribution regardless of their geometry and their base states as inherited from the compaction model. In addition, simulations reveal that local effects such as differences in relative density, residual stresses and geometry do not seem to significantly affect the final grain size and sintering time needed to densify ceramic compacts. An in-depth study of shear yielding and its relationship with compact cracking is needed to improve the current compaction model. The sintering model works reasonably well as shown with the density changes as a function of time in Figure 15.

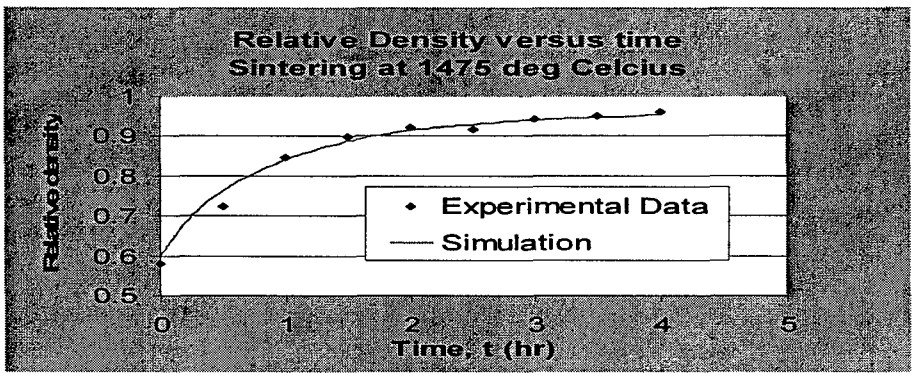

Figure 15: The density evolution predicted by simulation and measured experimentally.

3. Novel Processing techniques

3.1 Powder Preparation

Seven different powders, three types of alumina and four types of Partially-Stabilized Zirconia (PSZ) or zirconia, were used in this study. As will be explained further, many powders had to be mixed to control the residual stresses, which prematurely damage the samples during fabrication. Table 1 summarizes the average particle size and the manufacturers of the powders used in this study. The Coefficients of Thermal Expansion (CTEs) of alumina and zirconia are 8.1×10^{-6} and 10.0×10^{-6}/°C at a room temperature, respectively. However, such small difference in CTEs will cause the warpage when the bulk materials of alumina and zirconia are joined together at high temperatures and cooled to room temperature. Additionally, alumina and zirconia powders have a major difference in densification, which exhibits as the shrinkage difference. When they are processed together, premature damages such as cracks and distortion as shown in Figure 16 are prevalent. The sample shown in Figure 16 has three layers, zirconia and alumina and 50/50 mixture of the two powders.

In the fabrication of the samples, a uniaxial steel die was used to press all specimens in this study at the pressure of 35 MPa. In preparing multi-layered FGMs, various 'composite' powder mixtures of alumina and zirconia were prepared. In mixing the powders, the weight measurement of each constituent powders are used to calculate the volume fraction of the mixture based on their respective densities. A layer of one mixture, another layer of another mixture and so on were deposited layer by layer into the die and pressed to form the multi-layer FGMs. When the fugitive phases are embedded, the load has been reduced up to 50% to reduce the propensity of forming cracks in the samples.

Materials	Powder Name	Manufacturer	Average Particle Size (μm)
Alumina	TMDAR	Tamei, Japan	0.21
	AKP-50	Sumitomoto, Japan	0.1-03
	CR-15	Baikowski, U.S.A.	0.2 (Agglomerate)
(Partially Stablized) Zirconia	TZ3YS	Tosoh, Japan	0.59
	Cerac	Cerac, U.S.A.	1.23
	Nanbo-s	Nanbo, China	0.3
	Nanbo	Nanbo, China	0.3

Table 1: Powders used in this study

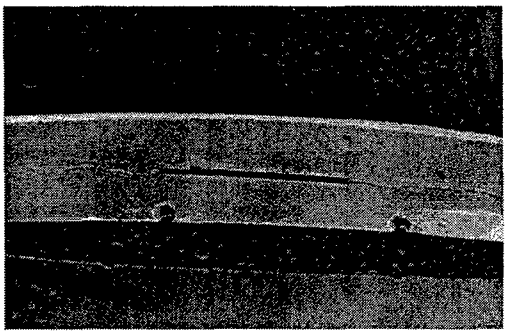

Figure 16: Multi-Layer FGMs with Cracks and Warpage

3.2 Controlling Residual Stress

Multi-layered FGM discs undistorted by process-induced residual stresses must be successfully produced to make the proposed efficient heat exchanger. The main problem that needed to be resolved was the fact that the zirconia powders shrink much more than alumina powder during sintering, exhibiting cracks in the processed multi-layer FGMs after sintering as demonstrated in Figure 16. To resolve this problem, first the shrinkage behavior of each powder individually must be understood. Thus, each powder was processed separately and the shrinkage after sintering has been measured. Our measurement in dimensions verifies that zirconia powders shrink substantially more than alumina powder except CR-15 after final sintering. Consequently, when the multi-layer FGMs are fabricated, the sintered samples warp. Alumina layer is in a state of compressive residual stress while the zirconia is in a state of residual tensile stress. The shrinkage from densification can be however controlled by manipulating the characteristics of the powder. As illustrated in Figure 17, this densification differential must also compensate the difference in the CTEs of alumina and zirconia. As finer powders can be nested within the interstitial spaces of larger powders, the final shrinkage can be reduced. This is a new technique to make FGMs undamaged by the process-induced residual stress, which was developed during the course of this research. As shown in McGeary's [1963] experiments with spherical particles, the diameter ratio between larger and smaller particles was 6.5:1. However, most commercially available powders had a size distribution and are not necessary spherical in shape. In this study, we have processed the powders with narrow size and wide size distribution. The narrow size distribution powder is attained using one type of powder while the wide size distribution powder was attained by mixing the powders with different sizes as Yeh and Sack [1988] had done.

To prove this concept, two zirconia powders, each with distinct average particle size, were obtained; Cerac and TZ3YS presented in Table 1. Again, the purpose of using two zirconia powders with distinct average particle size is to reduce the final shrinkage. The most severe configuration of FGMs in terms of residual stress is expected to be the two-layered FGMs, one with alumina and the other with zirconia. For the preliminary study, two-layer samples, one layer with TM-DAR and the other with various mixtures of TZ-3YS and CERAC powders, are pressed together and sintered at 1435°C. Because it is analytically impossible to determine the ideal mixture of Cerac and TZ3YS, the processing will allow us to determine this mixture ratio. Figure 18 shows the warpage (measured by the height ratio between the middle and edge) of the samples. The minimum warpage (less than 4% difference in height between the middle and edge) can be observed in the sample g which had the mixture ratio of 45% CERAC and 55% TZ-3YZ. However, the minute curvature could not be reduced further and any additional layer could not be successfully fabricated even after a series of extensive experiments.

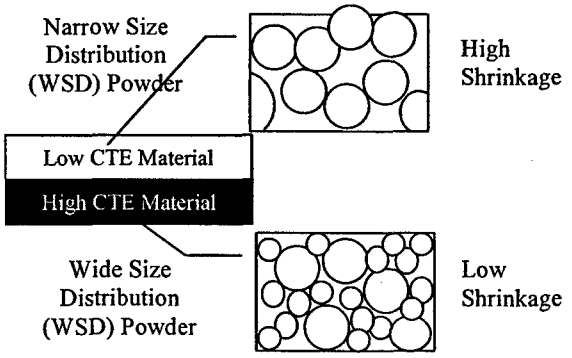

Figure 17: Shrinkage Control Using Different Powder Size Distribution.

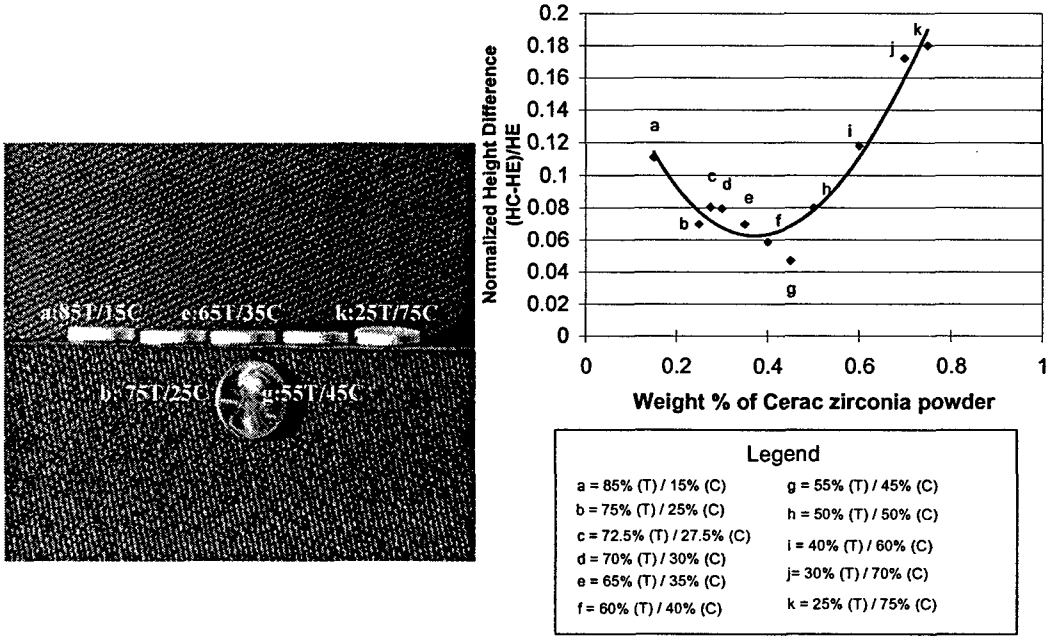

Figure 18: Eleven Samples With Alumina and Mixed Zirconia Showing Varying Degrees of Warpage.

We have expected that, once the ideal mixture was found, additional layers (composite between alumina and zirconia) between zirconia and alumina will expect to relieve the residual stress as they will form a more gradual gradient in FGMs. With the additional mixture layer, however, the minute warpage in the samples could not be completely eliminated. Therefore, additional powders such as Nanbo-s, Nanbo, AKP-50 and CR-15 powders was necessary to control the residual stresses even further. Nanbo and Nanbo-s are the smallest zirconia powder, which are expected to further reduce the shrinkage of zirconia layer. However, zirconia layer made with Nanbo powder usually cracked and Nanbo-s powder has been used for the rest of the processing. Because the TMDAR powder does compact so well, a possibility of using additional alumina powder is considered. However, if a powder with any substantial difference in average particle size is chosen, nesting of smaller powders within larger powders can results in smaller shrinkage in the alumina layer (as we are using this concept to minimize the shrinkage of zirconia). Thus, AKP-50 and CR-15, each with the average particle size of 0.2 micron (the same average particle size as TMDAR), are chosen. In the subsequent processing, sintering temperature was raised to 1475°C (higher than the sintering temperature used before). With the higher sintering temperature, a series of experiments has to be repeated to determine the ideal mixture for PSZ. From this experiment, the ideal mixture is found to be 40% Cerac and 60% TZ-3YS with less than 2% difference in height within the sample. CR-15 exhibits very high shrinkage to match the high shrinkage typical for zirconia powders, whose usage will be discussed in Sect. 3.8.

Using such trial-and-error method, three-layer and six-layer FGMs are also successfully fabricated. The mixture of 60% TMDAR/ 40% AKP-50 turns out to be the best mixture that matched the shrinkage of the mixture of 60% TZ3YS/ 40% Cerac. The ideal powder combinations are; the alumina layer has 60%TMDAR/40% AKP-50, 50/50 mixture of 50% TMDAR/50% Nanbo-S and finally the PSZ layer 60% TZ3YS/ 40% Cerac. Similarly six-layered FGMs with 25/75 and 75/25 mixtures of TMDAR and Nanbo-S have been also successfully fabricated as shown in Figure 8. These finding has been extended to fabricate different gradiency by controlling the thickness of each layers as were represented by Model 1 and Model 2 in Figure 2. The approach taken in this study provide a unique solution to many previous works reporting the problems due to the processing-induced residual stress in co-sintering multiple layers between zircnonia and alumina [Lee et al., 2002; Cai et al., 1997a, 1997b; Sorenen, 2002; Shinagawa and Hirashima, 2003]. These works have considered alternating layers or symmetric lay-up of alumina and zirconia where the work presented here represent the solution to both symmetric and non-symmetric lay-up of alumina and zirconia.

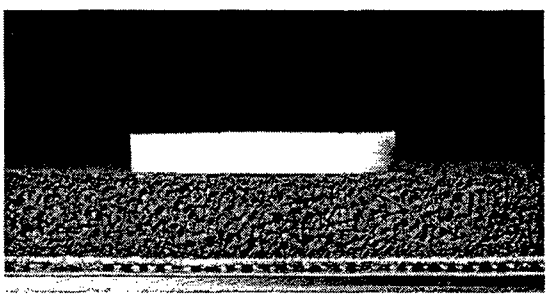

Figure 19: Equal-thickness (Model 1) 6-layered FGM without warping due to residual stress

3.3 Residual Stress Measurement

In the processing of FGMs, the residual stress has been managed to the point that it does not result in a permanent warping in the samples. However, the residual stress does exist in the FGM sample we have fabricated. The subcontract work to Dr. Mike Prime at Los Alamo National Laboratory has used the crack compliance method. This is a destructive method where a sample is incrementally separated with the strain gage mounted on the sample. In our case, the 1.07mm thick diamond wheel rotating 3600rpm has been used with the cutting depth of 1 micron meter per pass. The strain gage reads every 25 micro meter depth. Two FGM samples denoted Sample A and Sample B, were supplied. Sample A was cut from the zirconia side while the strain gage reading was measured. However, after cutting 25% of the complete cut, bonding to the fixture has separated and the test had to be stopped. Thus only the measurement to about 25% of thickness is available. Sample B was cut from the alumina side and the measurement was made completely. These measurements were presented in Figure 20.

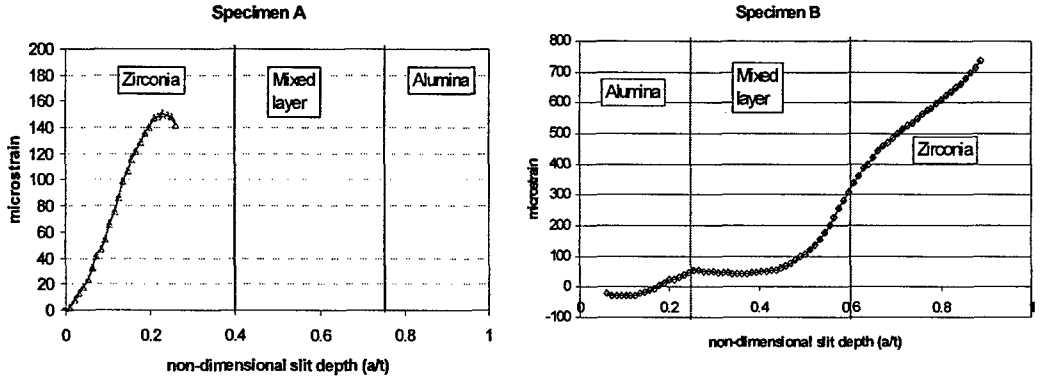

Figure 20: The Raw Data from the Strain gage

To interpret the raw data from the strain gages, elastic inverse problem was solved using superposition and series expansion inverse and a forward solution was implemented through FEM. The result shows saw-tooth residual stress as shown in Figure 13. Another method of measuring residual stress is contour method if the sample can be cleanly broken (brittle). We could possibly ABAQUS Python scripting interface to mesh actual part with a minute warping and straight slit for each cut depth and then get more accurate results but it requires significant effort. The results are for three-layered FGMs and the combined stress of operating stress shown in Figure 21 and the residual stress in Fig. 21 may reach close to the limited strength of materials. If it does, by increase the number of layer as in six-layered FGMs the residual stress is expected to drop.

3.4 Channels and Manifolds

A new technique to introduce surface [Lee et al., 2000] and internal channels were developed using a "fugitive compound" added to the ceramic powders during compaction. Among many fugitive phases used (many grades of polymers, papers and graphite), graphite is the only fugitive material that successfully introduce internal channels without any damage. For circular channels, pencil leads with nominal diameters of 700, 500 and 300 microns were sectioned into 1 cm to 1.5 cm lengths prior to embedding them in the ceramic power. Prior to pressing, placing the fugitive phase on top of the ceramic powder produces surface or external channels while embedding them in the ceramic powder produces internal channels. The presintering was

conducted in air for three hours in an electric furnace to burn out the fugitive phase, with an average heating rate of roughly 5°C per minute to 900°C, and then a cooling rate of 10°C per minute. During heating, the specimens were placed on a thin powder bed of the same material as the specimen being sintered. Figure 22 shows the channels on a ceramic composite processed with 75% TMDAR and 25%TZ-8YS (Fully Stablized Zirconia powder) and the fully sintered ceramic with the surface channels made after pre-sintering process.

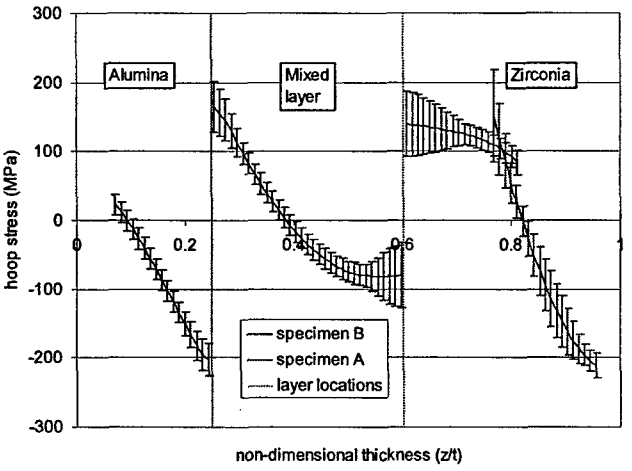

Figure 21: Residual Stress Estimation

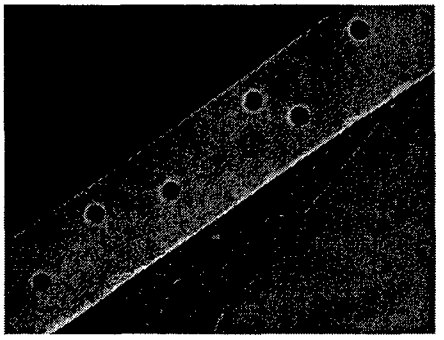

Figure 22: Multiple Internal Channels using Fugitive Phase.

3.5 Machining Pre-sintered Samples

As the shape of the channels becomes complex, powder flow around the complex fugitive phase becomes increasingly difficult. This leads to the formation of large cracks around the fugitive phase in the final ceramic parts. Most engineering ceramic materials after they have been fully sintered are too brittle and hard to machine with conventional machine tools. Mixing a binder phase with the powder is one way to avoid this problem. However, binder-burnout is undesirable due to the extended time requirement and the generation of toxic gases. Instead, we have prepared partially sintered ceramics (PSC) that have barely formed necks among the powders. PSC are easily handled and machined on a conventional table-top CNC machine. However, the processing variables are very sensitive to the processing conditions and a series of machining studies were necessary to determine optimal processing conditions. Figures 23 and 24 shows the differences in channel quality on zirconia pre-sintered at 600°C and 1000°C.

Based on the observations of zirconia, higher rpm (1500rpm), low feed rate (2.5mm/min) and pre-sintering above 800°C for 4 hrs are generally recommend. Figure 25 shows the collection of the quality of the channels on zirconia. Similar machining conditions (2000rpm and 2.5mm/min) are recommended for the pre-sintered alumina. However, the pre-sintering temperature of 600°C was much better. Figure 26 shows the machined complex channels after sintering.

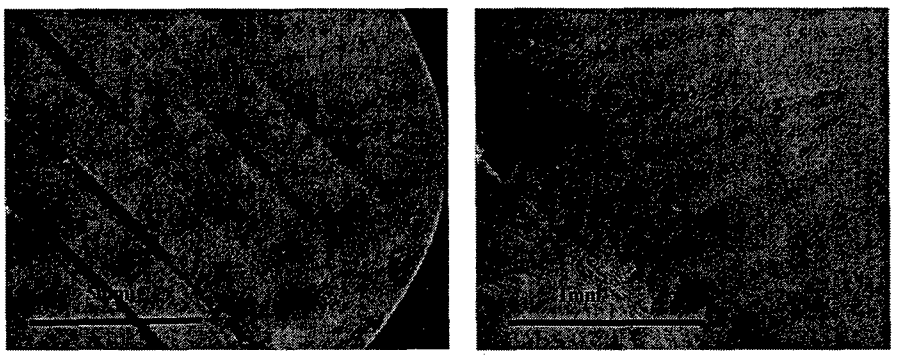

Figure 23: Pre-sintered Zirconia Sample at 600°C for 4 hr Milled at 500rpm and feed rate of 2.5, 5, 10, 15, 25 mm/min

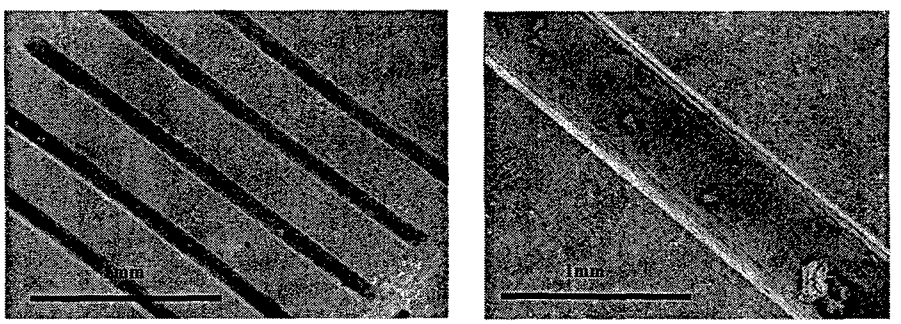

Figure 24: Pre-sintered Zirconia Sample at 1000°C for 4 hr Milled at 1500rpm and feed rate of 2.5, 5, 10, 15, 25 mm/min

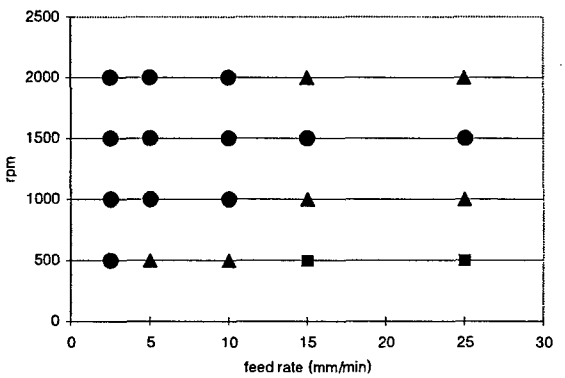

Figure 25: The Quality Measure (Excellent, ●, Good, ▲, Not Good, ■)of the Channels machined on Zirconia Pre-sintered at 1000°C.

Figure 26: Machined Pre-sintered Ceramics after Sintering with Complex Channel

3.6 Micro-Machining on Fugitive Phase

Another possible processing technique being explored is to extend the use of fugitive phase (graphite). Due to the excellent machinability of the graphite, the graphite has machined to provide the ribs that enhance mixing two fluids. Figure 27(a) shows the graphite whose cross section is 2mm by 2mm. The graphite sheet was cut using wire-EDM and micro-machined using a table-top CNC machine. Figure 27(b) shows the fully sintered sample embedded with the machined graphite that was fractured. The fabricated sample has been modeled using computational fluid dynamics code, Fluent 6.1. Prof. Shih at Iowa State University has provided the essential code fro his previous work [Shih et al., 2001], which was modified to simulate this model. Figure 28 shows the result of the simulation showing water and glycerin have mixed before reaching the end of channel with the inlet velocity of 0.5m/s. Because of the 3-dimensional arrangement of the ribs, the mixing takes place even for water and glycerin. The mixing channel may have a very important application such as micro-engine where the fuel and air has be mixed in a minute length scale before the mixture enters into a combustion chamber.

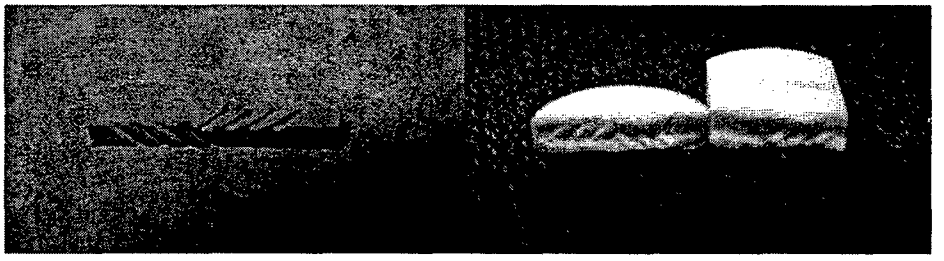

Figure 27: (a) The machined graphite and (b) the fractured sample.

3.7 Joining

We have successfully joined similar ceramics [Lee and Case, 1999] as well as dissimilar ceramics [Shin et al., 2000]. Joining technique can be used to join the samples with surface channels. After joining, the channels can be used to transport the coolants in and out of heat exchanger. In order to prepare the sintered specimen surfaces for joining, the surfaces to be joined were first polished and cleaned. Then a coating of amorphous silica was applied to the polished surfaces. The polishing was done with diamond paste having an abrasive size as small as one micron. The polished specimens were then ultrasonicated in a deionized water bath to help remove debris that accumulated during polishing. A coating of an organically-based silica precursor liquid was then spun onto the surfaces that were to be joined. The coatings were then converted into a thin (roughly 200 nm thick) layer of amorphous silica by heating the

coated specimen in air for approximately 20 minutes at 200°C. Joining was done at temperatures of roughly 1300°C - 1450°C using microwave or conventional furnace. Sintered disks with surface channels were joined with other disks to produce channels at the interface between the two components. Figure 29 shows the successful join (TZ-3YS and TZ-8YS) without precursor except one small section. Joining of pure alumina with other materials has not be consistently successful. Thus, this technique has not been utilized to make meso-scale heat exchangers.

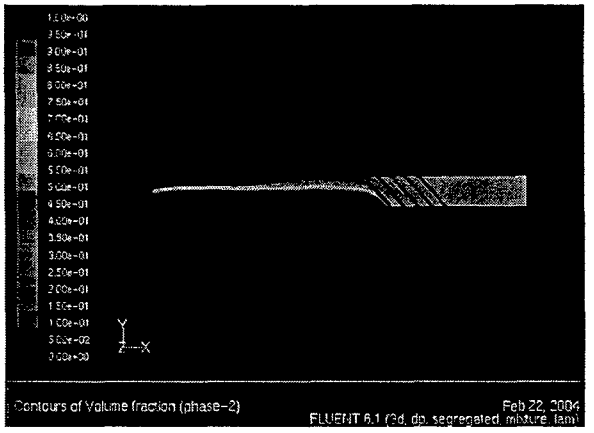

Figure 28: Mixing of Water and Glycerin after Introducing equal volumes at the Left Inlet

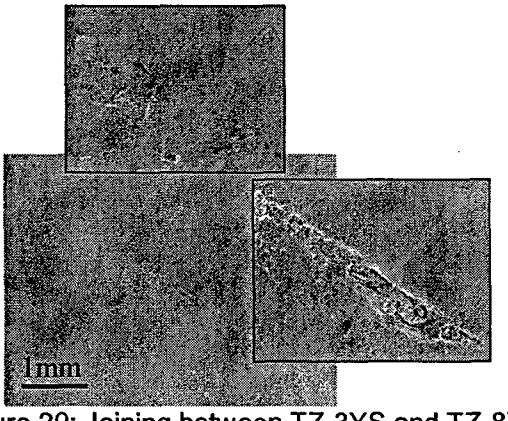

Figure 29: Joining between TZ-3YS and TZ-8YS

3.8 Meso-Scale Heat Exchanger

Three layered- FGM with channels has been successfully fabricated as shown in Figure 30. Even though there are some spots with agglomerations, the sample with channels was nearly flat without any warping or cracks. This sample represents FE Model 1 analyzed for the heat exchanger shown in Figure 2. Based on this success, we have attempted to fabricate much more complex geometry. The surface geometry for inlets and outlets that intended to connect through hoses was machined after partially sintered state of ceramics as shown in Figure 31. Figure 31(a) shows the illustrated image in UNIGRAPHICS and Figure 31(b) shows the fabricated heat exchanger. The crank-shape channels are made by milling the graphite sheet, which is pressed inside the powder compact. The compact is subsequently partially sintered at 700°C for 6 to 8 hours to burn out the graphite. The machining technique developed and presented

earlier has been used to make inlet and outlet using a small bench-top milling machine The same technique has been implemented to machine away the certain thickness of the top surface while leaving out four cylindrical protruded regions for the inlets and outlets. Each protruded region is then drilled from the top into the sample to make connection with the channels left out after partial sintering. This was successfully fabricated as shown in Fig. 30 for a homogeneous material. However, we could not successfully fabricate with the multi-layer FGMs. This may come from the powders which we have received within last six months. We suspect that the powder size and distribution and consequently compaction and sintering behavior may not be the same as the previous batches. Thus, the acquisition of additional alumina powder, CR-15, was necessary. This powder shrinks as much as the zirconia powder during sintering. With the addition of CR-15 in alumina, the multi-layer FGMs have been successfully produced.

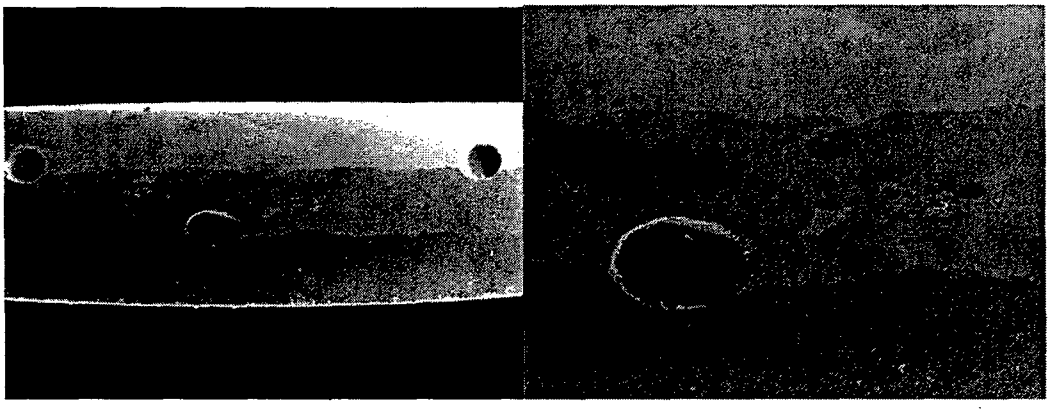

Figure 30: Three-layer FGMs with Channels

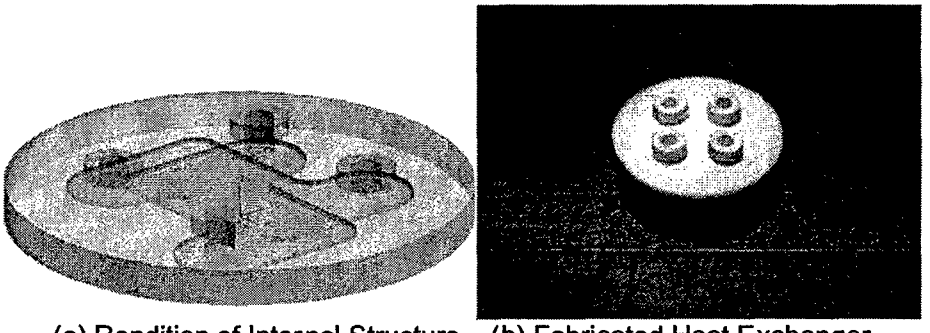

(a) Rendition of Internal Structure (b) Fabricated Heat Exchanger

Figure 31: Another Configuration of Heat Exchanger

4. Summary

Being able to micro-configure a ceramic material will impact the way we design and manufacture ceramic components. In addition, with the current research emphasis on micro-devices, we recognize that the immediate applications of the proposed processing techniques are in micro-heat exchangers for microelectronics, cryogenic surgery and cutting tools. Because of the inherent size of such a device, the effective use of materials is necessary. The key answer is in optimally texturing a material or materials by design based on a loading condition. That is the main motivation to use FGMs. The

most difficult problem with FGM is to control process-induced residual stress which damages the material before putting into use. The various processing methods introduced in this report has developed and improved. The combination of these processing methods has been adapted to fabricate the micro-textured and micro-configured meso-scale heat exchanger. Finally as shown in Figure 31, the prototype of meso-scale heat exchanger has been produced. Because powder processing is the main shaping process, we have developed compaction and sintering models to understand the intertwined functionality existing among various powder characteristics, processing conditions and corresponding shrinkage and densification behaviors.

References

Aydin, I., Briscoe, B. J. and Sanliturk, K.Y., 1996, Powder Technology, 89, pp. 239-254.

Bouvard, D. et al., 2002, Key Engineering Materials, 206-213, 243-248

Cai, P. Z., Green, D. J. and Messing, G. L., 1997a, *J. Am. Ceram. Soc.*, 80, 8, pp. 1929-1939.

Cai, P. Z., Green, D. J. and Messing, G. L., 1997b, *J. Am. Ceram. Soc.*, 80, 8, pp. 1940-1948.

Kim, K.T., Choi, S.W. and Park, H., 2000, Journal of Engineering Materials and Technology, **122**, 238-244.

Kim, H. G., Lee, H. M., and Kim, K. T., 2001, Journal of Engineering Materials and Technology, **123**, 221-228.

Kwon, Y. S. and K. T. Kim, 1996, Journal of Engineering Materials and Technology, **118**, pp. 448-455.

Kwon, P., Dharan, C.K.H., and M. Ferrari, 1994, J. Energy Res. Tech., **116**, p. 115.

Kwon, P. and Dharan, C.K.H., 1995, ASME Winter Annual Meeting, San Francisco, California.

Lee, K. Y. and Case, E., 1999, Materials Science and Engineering, A269: 8 - 20.

Lee, J. G., Case, E., Shin, H. and Kwon, P., 2000, Ceramic Engineering and Science Proceedings, 103 - 110.

Lee, J. G., Shin, H. W., Case, E., Kwon, P., 2001, J. Mat. Sci. Let., 20, 2, pp. 107-109.

McGeary, R. K., 1961, J. Am. Ceram. Soc., **44**, 10, pp. 613-522.

Shin, H.W., Case, E.D., Kwon, P and, Kok, C.K., 2002, Transactions of the American Ceramic Society, Westerville, OH.

Shinagawa, K. and Hirashima, Y., 2003, Key Engineering Materials, **233-23,** 6, pp. 785-790.

Sorenson, B. F., 2002, J. Am. Ceram. Soc., **85**, 4, pp. 858-864.

Ting, T. -M. and Lin, R. Y., 1994, J. Mat. Sci., pp. 1867-1872.

Ting, T. -M., and Lin, R. Y., 1995, J. Mat. Sci., pp. 2382-2389.

Yeh, T. and Sacks, M. D., 1988, J. Am. Ceram. Soc., **71**, 12, pp. C484-V487.

Zeuch, D. H, Grazier, J. M., Arguello, J. G., Ewsuk, K. G., 2001, Journal of Material Science, **36**, 2911-2924

Zipse, H., 1997, Journal of European Ceramic Society, 17, pp. 1707-1713.

Accomplishments/New Findings

- Machining Ceramics at Pre-sintered State
- Internal channels in the bulk of Ceramics using Fugitive Phase
- Joining Ceramics
- Processing of Multi-layered Functionally Graded Materials without warping due to process-induced residual stress

- Compaction Process Model
- Sintering Process Model
- Design of Meso-scale Heat Exchanger
- Fabrication of Meso-scale Heat Exchanger

Personnel Supported

Patrick Kwon and Eldon Case
Hyeaweon Shin (Ph.D. Student),
Chee Kong Kok (Ph.D. Student)
Ru Wang (Ph.D. Student)
Ren Fei (Ph.D. Student)
Ram Subramanian (M.S. Student)
Bejier Brooks (Mater Student)
Kyle Sutton (Undergraduate Student)
Dale Smith (Undergraduate Student)
Mark Lepech (Undergraduate Student)
Teresa Franklin (Undergraduate Student)
Ben Souder (Undergraduate Student)
Dennis Sumanski (Undergraduate Student)

Publications

H.W. Shin, P. Kwon and Case, E., 2002, "Novel Powder Processing Techniques of Efficient Meso-scale Heat Exchanger," Transactions of NAMRII/SME, v. XXX, pp. 671-679.

H.W. Shin, E.D. Case, P. Kwon, C.K. Kok, 2002, "Joining Zirconia and Alumina Bioceramics," Transactions of the American Ceramic Society, Westerville, OH.

P. Kwon, C. K. Kok, D. Fickes, C. W. Somerton, H. W. Shin and E. D. Case, 2002, "Processing Issues in Fabricating Ceramic Micro-Heat Exchangers by Joining Components," Transactions of the American Ceramic Society, Westerville, OH.

E. Case and P. Kwon, 2003, "Machining and Joining of Specimens with Meso-scale Channels," Advanced Ceramics Meeting, Cocoa Beach, FL.

H. Shin, E. Case and P. Kwon, 2003, "The Fabrication of Internal Channels in Ceramics and Ceramic Composites," Journal of Advanced Materials, 35, 2, pp. 28-35.

C. K. Kok and P. Kwon, "Processing Models for making Meso-scale Heat Exchangers" submitted to NAMRC XXXII, University if North Carolina, Charlotte.

H. Shin, P. Kwon and E. Case, 2003, "Meso-Scale Channels On Ceramics By Machining," 2003 Winter Topical Meeting, Machines And Processes For Micro-Scale And Meso-Scale Fabrication, Metrology And Assembly, ASPE, Gainesville, Florida

C. K. Kok, P. Kwon, B. Klenow and R. Rachedi "Finite-Element Simulation of the Uniaxial Die Pressing of Ceramic Powder," ASPE 18th Annual Meeting, Portland, OR, (2003).

H. Shin, C. Kok, P. Kwon and E. Case, 2004, "Meso-scale channels on Ceramics by Machining," Journal of Manufacturing Processes, **6**, 1, pp. 15-23.

E. Case, P. Kwon, R. Fei, C. Kok, B. Klenow and R. Rachedi, 2004, "Machining and ceramic/ceramic joining to form internal meso-scale channels," Journal of Applied Ceramic Technology, **1**, 1, pp. 95-103.

C.K. Kok and P. Kwon, 2004, "Compaction Models for Ceramic Powder in Making Meso-Scale Heat Exchangers," Transaction of NAMRII XXXII, pp. 423-430.

R. Subramanian and P. Kwon, 2004, "Design of an Efficient Active Cooled Meso-Scale Heat Exchanger Using Functionally Gradient Materials," ASPE, Orlando, FL.

Z. C. Li, Z. J. Pei, W. M. Zeng, P. Kwon and C. Treadwell , 2004, "Experimental Study of Cutting Force In Rotary Ultrasonic Machining On Zirconia Toughened Alumina," Transaction of NAMRII/SME, XXXI

B. K. Paul, P. Kwon and R. Subramanian, 2005, "Limits on Aspect Ratio in Two-Fluid Micro-Scale Heat Exchangers," ASME Transactions, Journal of Manufacturing Science and Engineering, revision submitted.

T. Franklin and P. Kwon, 2005, "Minimizing Process-Induced Residual Stress in Multi-Layer Materials," submitted to ASME Transactions, Journal of Manufacturing Science and Engineering, **also** JSME/ASME International Conference on Materials and Processing.

Interactions/Transactions

P. Kwon, 2002, presentation at NAMRI/SME Conference, West Lafayette, IN.
P. Kwon, 2002, presentation at UKC-2002, Seoul, Korea.
P. Kwon, 2002, interactions with Ralph Resnick and Dan Mass about the possibility of using 3-D Printing Unit for Deposition of Powders, Extrude Hone Corporation.
P. Kwon, 2003, presentation at ASPE Winter Topical Meeting, Gainesville, FL.
P. Kwon, 2003, presentation at AFOSR Contractors' Meeting , Santa Fe, New Mexico.
P. Kwon, 2004, presentation at NAMRI, Charlotte, NC.
P. Kwon, 2004, presentation at AFOSR Contractors' Meeting, Wintergreen, VA.
P. Kwon, 2004, presentation at Naval Research Lab., Washington DC.
P. Kwon, 2005, presentation at NAMRI, New York, NY.
P. Kwon, 2005, presentation at AFOSR Contractors' Meeting, Sante Fe, NM.
P. Kwon, 2005, presentation at JSME/ASME International Conference on Materials and Processing.

New Discoveries, Inventions or Patent Disclosure

None.

Honors/Awards

None.